

Case C1.4: Laminar Boundary Layer on a Flat Plate

Masayuki Yano* and David L. Darmofal†

Aerospace Computational Design Laboratory, Massachusetts Institute of Technology

I. Code Description

ProjectX is a high-order, adaptive discontinuous Galerkin finite element solver. The DG discretization uses Roe’s approximate Riemann solver¹ for the inviscid numerical flux and Bassi and Rebay’s second discretization (BR2)² for the viscous numerical flux. The solution to the discretized system is obtained using a Newton-based nonlinear solver with pseudo-time continuation; however, due to the simplicity of this case, we employ a very high CFL number (10^6) to achieve near-Newton convergence (except on the very first solve of the adaptation sequence). The linear system arising in each pseudo-time step is solved using GMRES,³ preconditioned with an in-place block-ILU(0) factorization⁴ with minimum discarded fill reordering and $p = 0$ algebraic coarse correction.⁵

An output-based, anisotropic simplex adaptation algorithm is used to control the discretization error.⁶ The algorithm iterates toward a mesh that minimizes the output error for a given number of degrees of freedom. The anisotropic adaptation decisions are entirely driven by the behavior of an output-based *a posteriori* error estimate; thus, the method handles any discretization order, naturally incorporates both the primal and adjoint solution behaviors, and robustly treats irregular features. The output error estimate uses the dual-weighted residual (DWR) method of Becker and Rannacher.⁷ A new mesh that conforms to the metric request is generated using using BAMG (Bidimensional Anisotropic Mesh Generator).⁸

II. Case Description

II.A. Flow Condition

This case considers subsonic, laminar flow over a flat plate. The freestream Mach number is $M_\infty = 0.5$, and the Reynolds number based on the plate length is $Re_L = 1 \times 10^6$. A constant viscosity is used throughout the domain, and the Prandtl number is set to $Pr = 0.72$.

II.B. Domain Specification

The flat plate geometry is parametrized by two parameters, L_H and L_V , as provided in the problem description. A sensitivity study of the drag against the domain parameters is performed, where we have chosen for simplicity

$$L_H = L_V = R,$$

where R is the single parameter controlling the domain size. Figure 1 shows the result of the sensitivity study. Each solution is obtained using the adaptive $p = 3$, $dof = 20000$ discretization, which results in the c_d error of less than 10^{-9} ; thus each solution is grid converged (for the purpose of this sensitivity study) and the c_d variation is solely due to the difference in the farfield location. The result suggests that $R = 1.0$ is sufficient to meet the required c_d variation of less than 0.01 counts. Thus, for the rest of this case, the domain parameters are set to $L_H = L_V = 1.0$.

*Doctoral candidate, 77 Massachusetts Ave. 37-442, Cambridge, MA, 02139, myano@mit.edu

†Professor, 77 Massachusetts Ave. 37-451, Cambridge, MA, 02139, darmofal@mit.edu

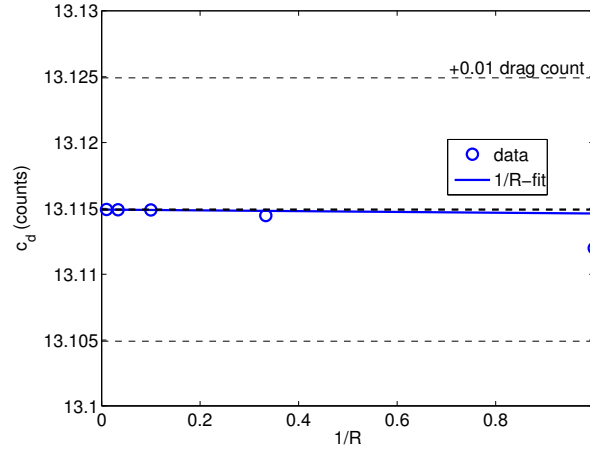


Figure 1. The sensitivity of the drag coefficient on the farfield location.

II.C. Convergence Criterion

The ℓ^2 norm of the DG residual of non-dimensionalized Navier-Stokes equations is used to monitor convergence to the steady state. Our solver operates on non-dimensionalized variables

$$\rho^* = \frac{\rho}{\rho_\infty}, \quad u^* = \frac{u}{\|V_\infty\|}, \quad v^* = \frac{v}{\|V_\infty\|}, \quad p^* = \frac{p}{\rho_\infty \|V_\infty\|^2}, \quad e^* = \frac{e}{\|V_\infty\|^2},$$

$$R^* = \frac{R}{c_v}, \quad T^* = \frac{T}{\|V_\infty\|^2 / c_v}, \quad \text{and} \quad \mu^* = \frac{\mu}{\rho_\infty L_\infty V_\infty}.$$

The DG residual is computed against the Lagrange test functions with equidistributed nodes, and the ℓ^2 norm of the residual is converged to 1×10^{-10} . (Note that the solver time would not be significantly influenced for any reasonable choice of the tolerance (say $< 1 \times 10^{-7}$), as we achieve Newton convergence in this regime. With the specified non-dimensionalization, the difference between the ℓ^2 residual and the mass residual is well within this offset.)

II.D. Hardware Specification

All computations are performed in serial on a Linux machine with an Intel i7-2600 processor and 16 Gbytes of RAM. The machine produces a Taubench time of 6.60 seconds.

II.E. Residual Timing

The time for performing a single dof = 250,000 residual evaluation, including the full Jacobian for the implicit solver, is summarized in Table 1. The residual evaluation is performed on a 5768-element mesh and the times are scaled to 250,000 degrees of freedom.

p	time (work unit)
1	0.82
2	0.80
3	0.94

Table 1. dof = 250,000 residual evaluation time (including the full Jacobian construction).

II.F. Initial Mesh

The initial mesh used for this flat plate case is shown in Figure 2. Unlike initial meshes used for the other workshop cases, the initial mesh for this case is refined toward the boundary layer. This refinement is necessary to facilitate the nonlinear solver convergence; because the flow has a high Reynolds number but

is laminar, the mesh-induced perturbation makes the flow unsteady when the flow features are significantly underresolved. However, note that the initial mesh is not refined in the leading edge region.

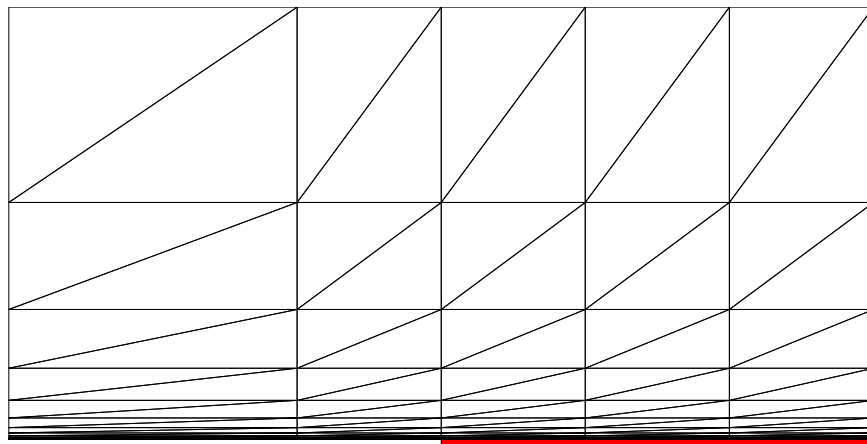


Figure 2. The initial 150-element mesh. The flatplate region is marked in red.

II.G. Adaptation Procedure and Data Reported

The range of the discretization orders, p , and the degrees of freedom, dof, considered for this case are

$$p \in \{1, 2, 3\} \quad \text{and} \quad \text{dof} \in \{500, 1000, 2000, 4000\}.$$

For each p -dof combination, a family of optimized meshes are generated using our anisotropic simplex mesh adaptation algorithm.⁶ The output adapted is the drag on the plate.

As in Case 1.1, the performance of each p -dof is assessed by averaging the error obtained on five realization of meshes in the family. The time reported is the total time required to reach the first realization of the p -dof-optimized mesh starting from the initial mesh shown in Figure 2; this includes multiple flow solves and adaptation overhead. (See the description provided in Case 1.1 for details.)

III. Results

III.A. Error Convergence

The reference solution is obtained using the adaptive $p = 3$, dof = 20000 discretization. The reference c_d value used for the case is

$$c_d = 0.00131119952 \pm 4 \times 10^{-11}$$

where the error estimate is provided based on the adjoint-based error estimate and the fluctuation in the c_d value for this family of optimized meshes.

The c_d error convergence against the number of degrees of freedom is shown in Figure 3(a). Note that, if the problem is smooth, the expected output error convergence rate using a dual-consistent discretization for a viscous problem in two dimensions is

$$\mathcal{E} = Ch^{2p} = \tilde{C}(\text{dof})^{-p}.$$

The figure shows that the adaptive algorithm achieves the optimal convergence rate despite the presence of singularity at the leading edge. With the effective control of the singularity through mesh refinement, the $p > 1$ discretizations require fewer degrees of freedom than the $p = 1$ discretization for error level of approximately 0.01 drag counts or less. We also note that the c_d error is less than 0.1 counts, even on the coarsest meshes with 500 degrees of freedom, e.g. the adaptive $p = 3$ discretization achieves less than 0.1 counts of error using only 50 elements.

The result of the c_d convergence against the work unit is shown in Figure 3(b). The longer time required for $p > 1$ for a given degrees of freedom is due to a larger number of adaptation iterations required to reach

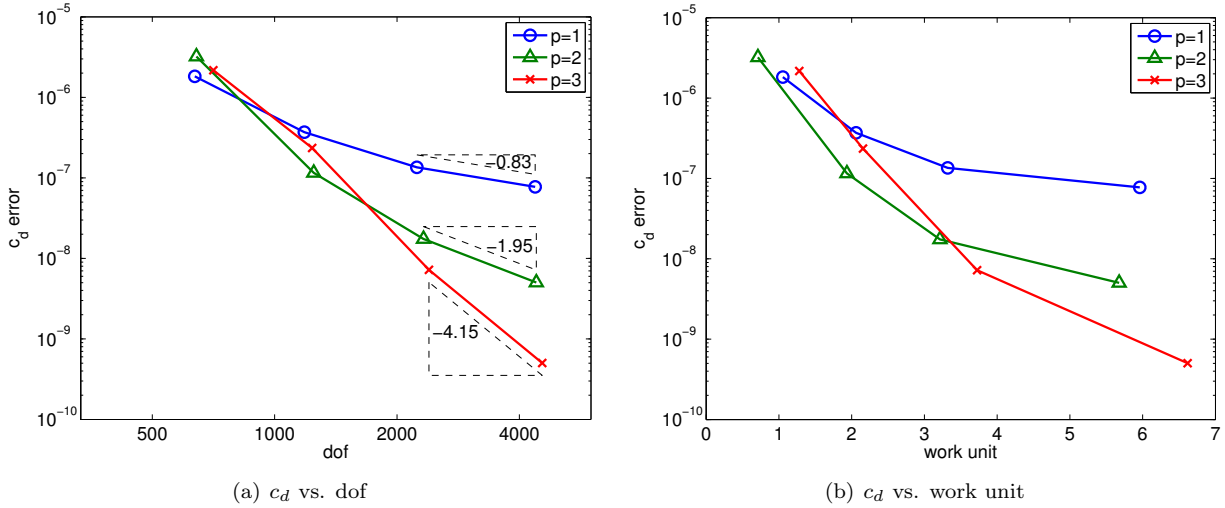


Figure 3. Drag error convergence.

a p -dof optimal mesh that controls the effect of the singularity. (For a given degrees of freedom, our flow solver in fact runs faster for a higher p .) Again for simulations requiring accuracy of less than 0.01 drag counts, the $p > 1$ discretizations are more efficient than the $p = 1$ discretization.

III.B. Comparison of Adapted Meshes

Drag-adapted meshes obtained for select p -dof combinations are shown in Figure 4. In general, adaptive refinement targets the boundary layer and the leading edge singularity. Isotropic elements are used to resolve the leading edge singularity, whereas anisotropic elements with are used in the boundary layer region. The aspect ratio of the elements in the boundary layer region is as high as 1,000.

Comparison of the $p = 1$, dof = 4,000 mesh (Figure 4(a)) and the $p = 2$, dof = 1,000 mesh (Figure 4(b)) reveals the differences in the meshes required to achieve the drag error level of 10^{-7} using the $p = 1$ and $p = 2$ discretizations. The $p = 2$ mesh is significantly sparser in the freestream region and in the boundary layer. Because the boundary layer is a smooth feature (i.e. results from singular perturbation and is not a singularity), the higher-degree polynomial is very effective at resolving the feature.

Comparison of the $p = 2$, dof = 1,000 mesh (Figure 4(b)) and the $p = 2$, dof = 4,000 mesh (Figure 4(c)) shows how the mesh evolves for a given p to achieve a lower error level (or as the number of degrees of freedom increases). In increasing the available number of degrees of freedom by a factor of four, the diameter of the leading edge element decreases from $h_{le} \approx 7 \times 10^{-4}$ to 3×10^{-5} , i.e. the leading edge element diameter decreases by a factor of over 20, whereas uniform refinement would have resulted in the diameter decreasing by a factor of two. The refinement is clearly not uniform, and adaptation targets the leading edge singularity.

III.C. Adaptive vs. Uniform Refinement

Figure 5 compares the convergence results obtained using adaptive refinement and a step of uniform refinement starting from select adapted meshes. Due to the presence of the leading edge singularity, uniform refinement results in suboptimal convergence, even though the mesh from which uniform refinement is performed has been optimized for a lower number of degrees of freedom. This simple problem highlights the importance of performing mesh adaptation and controlling the effect of singularities, especially for high-order discretizations.

Acknowledgments

The authors would like to thank the entire ProjectX team for the many contributions that enabled this work. This work was supported by the Singapore-MIT Alliance Fellowship in Computational Engineering and The Boeing Company with technical monitor Dr. Mori Mani.

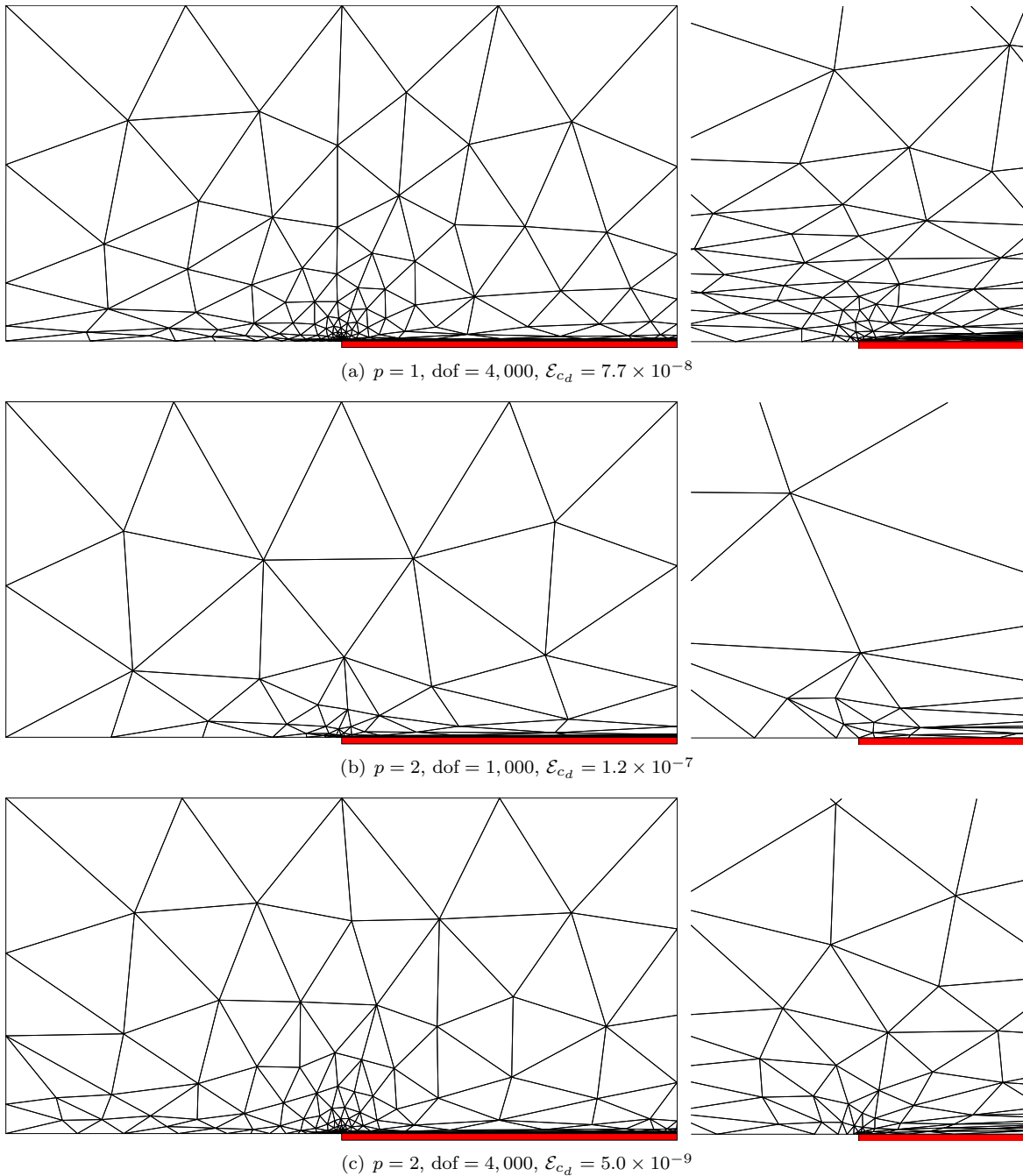


Figure 4. Select drag-adapted meshes. The overview (left) and the zoom in the region $[-\delta/2, \delta/2] \times [0, \delta]$ with $\delta = 10^{-2}L$.

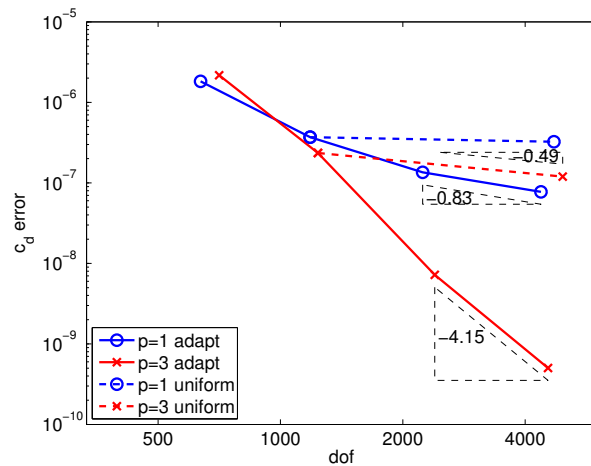


Figure 5. Comparison of adaptive refinement and uniform refinement starting from adapted meshes.

References

- ¹P. L. Roe, Approximate Riemann solvers, parameter vectors, and difference schemes, *J. Comput. Phys.* 43 (2) (1981) 357–372.
- ²F. Bassi, S. Rebay, GMRES discontinuous Galerkin solution of the compressible Navier-Stokes equations, in: K. Cockburn, Shu (Eds.), *Discontinuous Galerkin Methods: Theory, Computation and Applications*, Springer, Berlin, 2000, pp. 197–208.
- ³Y. Saad, M. H. Schultz, GMRES: A generalized minimal residual algorithm for solving nonsymmetric linear systems, *SIAM Journal on Scientific and Statistical Computing* 7 (3) (1986) 856–869.
- ⁴L. T. Diosady, D. L. Darmofal, Preconditioning methods for discontinuous Galerkin solutions of the Navier-Stokes equations, *J. Comput. Phys.* 228 (2009) 3917–3935.
- ⁵P.-O. Persson, J. Peraire, Newton-GMRES preconditioning for discontinuous Galerkin discretizations of the Navier-Stokes equations, *SIAM J. Sci. Comput.* 30 (6) (2008) 2709–2722.
- ⁶M. Yano, D. Darmofal, An optimization framework for anisotropic simplex mesh adaptation: application to aerodynamic flows, *AIAA 2012-0079* (Jan. 2012).
- ⁷R. Becker, R. Rannacher, An optimal control approach to a posteriori error estimation in finite element methods, in: A. Iserles (Ed.), *Acta Numerica*, Cambridge University Press, 2001.
- ⁸F. Hecht, Bamg: Bidimensional anisotropic mesh generator, <http://www-rocq1.inria.fr/gamma/cdrom/www/bamg/eng.htm> (1998).